

Forward Rapidity Results from RHIC

I.G. Bearden^g, D. Beavis^a, C. Besliu^j, B. Budick^f, H. Bøggild^g, C. Chasman^a, C. H. Christensen^g, P. Christiansen^g, J. Cibor^c, R. Debbé^a, E. Enger^l, J. J. Gaardhøje^g, M. Germinario^g, K. Hagel^{h,*}, O. Hansen^g, A. Holm^g, A. K. Holme^l, H. Ito^{k,a}, A. Jipaⁱ, F. Jundt^b, J. J. Jørdreⁱ, C.E.Jørgensen^g, R. Karabowicz^d, E. J. Kim^{a,k}, T. Kozik^d, T. M. Larsen^l, J. H. Lee^a, Y. K. Lee^e, G. Løvholden^l, Z. Majka^d, A. Makeev^h, M. Mikelsen^l, M. Murray^{h,k}, J. Natowitz^h, B. S. Nielsen^g, J. Norris^k, K. Olchanski^a, D. Ouerdane^g, R. Płaneta^d, F. Rami^b, C. Ristea^j, D. Röhrichⁱ, B.H. Samset^l, D. Sandberg^g, S.J. Sanders^k, R.A. Scheetz^a, P. Staszal^{g,d}, T.S. Tvetter^l, F. Videbæk^a, R. Wada^h, Z. Yinⁱ, and I. S. Zgura^j

The BRAHMS Collaboration

^a Brookhaven National Laboratory, Upton, New York 11973.

^b Institut de Recherches Subatomiques and Université Louis Pasteur, Strasbourg, France.

^c Institute of Nuclear Physics, Krakow, Poland.

^d Smoluchowski Inst. of Physics, Jagiellonian University, Krakow, Poland

^e Johns Hopkins University, Baltimore 21218.

^f New York University, New York 10003.

^g Niels Bohr Institute, Blegdamsvej 17, University of Copenhagen, Copenhagen 2100, Denmark

^h Texas A&M University, College Station, Texas, 17843

ⁱ University of Bergen, Department of Physics, Bergen, Norway.

^j University of Bucharest, Romania.

^k University of Kansas, Lawrence, Kansas 66045.

^l University of Oslo, Department of Physics, Oslo, Norway

Recibido el 29 de enero de 2005; aceptado el 12 de marzo de 2005

A summary of BRAHMS results is presented. Emphasis is placed on data for which measurements at forward rapidities are necessary for interpretation. This includes measurements of spectra over a wide range of y and transverse momentum, yields, stopping, quark chemistry and high p_t suppression in both Au+Au and d+Au collisions at $\sqrt{s_{NN}} = 200$ GeV.

Keywords: Quark chemistry; rapidity density; stopping; high p_t suppression.

Se presenta un resumen de los resultados obtenidos en BRAHMS, enfatizando en aquellos datos cuya interpretacion requiere las medidas de las rapideces. Esto incluye mediciones del espectro sobre un amplio rango de "y" y momento transverso, productos, frenados, quimica de cuarks y alta supresion de P_t en colisiones de Au + Au y d + Au a $\sqrt{s_{NN}}=200\text{GeV}$.

Descriptores: Química de cuarks; densidad de rapideces; frenado; alta supresion p_t .

PACS: 25.70.Pq; 24.60.Ky; 05.70.Jk

1. Introduction

Detailed measurements over a wide region of phase space are very important in understanding possible new states of matter at RHIC energies where $\sqrt{s_{NN}} = 200$ GeV. BRAHMS has the unique capability of providing detailed high resolution information from mid-rapidity to a rapidity as high as 4.

In this contribution we summarize the results of various measurements over a large region of phase space using BRAHMS. We focus on the measurements where the particular characteristics of BRAHMS can be exploited to obtain unique information. Based on measurements of particle multiplicity, the initial energy density can be estimated. Measurements of particle composition can provide information on the quark chemistry of the hot dense matter over a large range of rapidity. Our study of the net baryon distribution in Au + Au collisions allows the extraction of energy loss per participant. Finally, the suppression of high p_t particles has been studied in Au+Au and d+Au as a function of rapidity and centrality, to disentangle effects related to the hot dense final system and

to the initial conditions of Au nuclei before collisions.

Aside from measurements with the global detectors, all of the measurements presented are derived from the identified particle transverse momentum spectra for $0 < y < 3.2$ which, after suitable fitting, lead to the measured yields. Unless otherwise noted, the data shown are from the 5% most central collisions. A description of the experimental setup can be found in [1].

2. Global Multiplicity Distributions

BRAHMS employs a series of global detectors in order to characterize overall properties of the measured reactions as well as to determine the collision vertex [1]. These detectors also have the capability of providing a measure of the multiplicity of unidentified charged particles. Such measurements are important because they can constrain models [2,3] by providing information on hadronic rescattering, the degree of chemical and thermal equilibrium and the role of partonic processes. Such data can also provide information on the en-

ergy density of the system [4]. Figure 1 shows the multiplicity distributions for collisions with centralities ranging from 0-5% to 40-50%. We note that at $\eta \approx 0$ the 5% most central collisions have a $dN/d\eta \approx 625$. The integral of the multiplicity distribution in the 0-5% most central collisions is ~ 4600 .

To use these multiplicities to estimate the energy density, we employ [4]

$$\epsilon \approx \frac{1}{\pi R^2 \tau} \frac{d\langle E_t \rangle}{dy} = \frac{\langle m_t \rangle}{\pi R^2 \tau} \frac{dN}{dy} \quad (1)$$

Taking the formation time, $\tau \sim 1$ fm/c, R as the radius of the overlap disk of the colliding nuclei and m_t determined from rapidity densities and average transverse momenta measurements (discussed later), $\epsilon \approx 5$ GeV/fm³. It is noted that this value, which should be considered as a lower limit, exceeds the QGP production threshold predicted by QCD calculations by a factor of 5 [5, 6].

At forward rapidity, the multiplicity distributions are shown, however, to be independent of collision centrality and beam energy when scaled by number of pairs of participating nucleons. Figure 2 shows the scaled multiplicity distributions as a function of the difference between the pseudo-rapidity, η , and the beam rapidity. We observe a consistency even between our data and data at $\sqrt{s_{NN}} = 17$ GeV [7] in the region where η is between 0.5 and ~ 1.6 units less than the beam rapidity. This observation is consistent with a limiting fragmentation picture in which the excitation of the fragment baryons near the beam rapidity, y_B , depends on how far they are from y_B and is independent of system size [8].

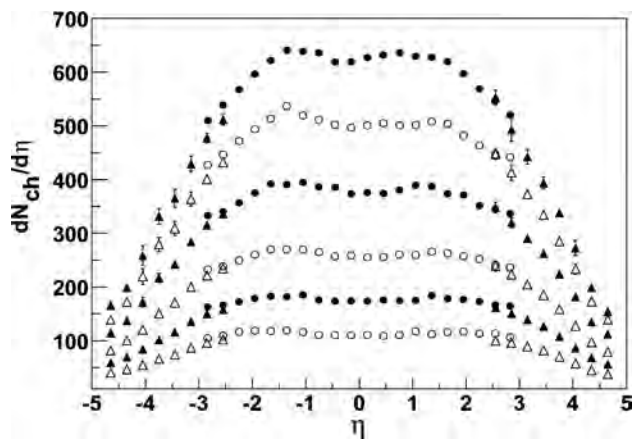


FIGURE 1. Multiplicity distributions, $dN/d\eta$ for centralities ranging from 0-5% (top distribution) to 40-50% (bottom distribution). The central rapidity region, $\eta < 2.5$, represented by open and closed circles, shows the distributions measured with the Silicon and Tile Multiplicity arrays [1] and the forward region, represented by the open and closed triangles, shows the distributions measured with the Beam-Beam Counters [1]. Statistical errors are shown whenever larger than the symbol size.

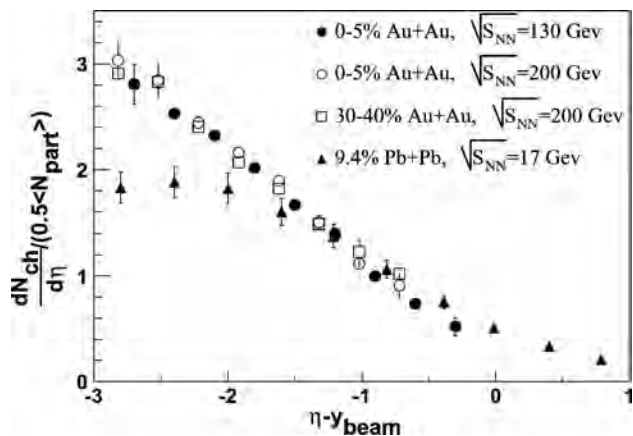


FIGURE 2. Charged particle multiplicities scaled to the number of participating nucleon pairs as a function of η shifted by the beam rapidity. The meaning of the symbols is shown in the figure.

3. Spectra and Yields

We have produced differential transverse momentum (p_t) spectra of positive and negative pions, kaons and protons. The negative particle π , K and p spectra transformed into transverse mass, $m_T = \sqrt{p_t^2 + m^2}$, are shown in Fig. 3 for the different measured rapidities ranging from $y \approx 0$ to $y \approx 4$. We note that the shapes of the spectra depend on the species. The various spectra were fit with different functions in transverse momentum, p_t or transverse mass, $m_t = \sqrt{p_t^2 + m^2}$, depending on the shape of the spectrum of a given particle. The pion spectra were fit with a power law, $(1 + p_t/p_0)^{-n}$, the kaon spectra with an exponential, $\exp[(m_t - m)/T]$ and the proton spectra with a Gaussian, $\exp(-p_t^2/2\sigma^2)$. The dashed lines in Fig. 3 show the fits to the various spectra.

From the fits one can extract the yields by integrating the appropriate functions over the entire m_t range. This gives the rapidity densities shown in the upper panel of Fig. 4. The positive and negative pions show nearly the same distribution over the entire rapidity range measured while the anti-protons show a decrease as the rapidity approaches the beam rapidity in contrast to the protons which remain rather constant.

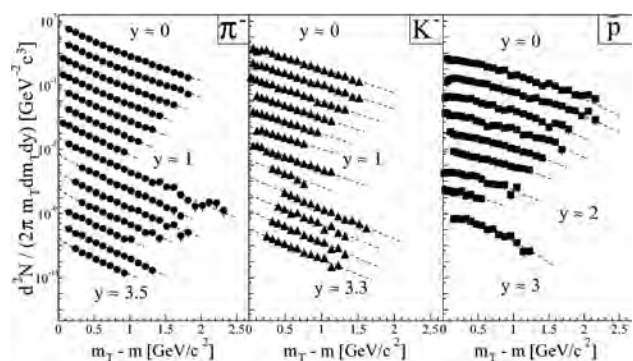


FIGURE 3. $m_t - m$ for π^- , K^- and \bar{p} spectra from Au+Au at $\sqrt{s_{NN}} = 200$ GeV at different rapidities. The lines indicate the different fits to the data (see text).

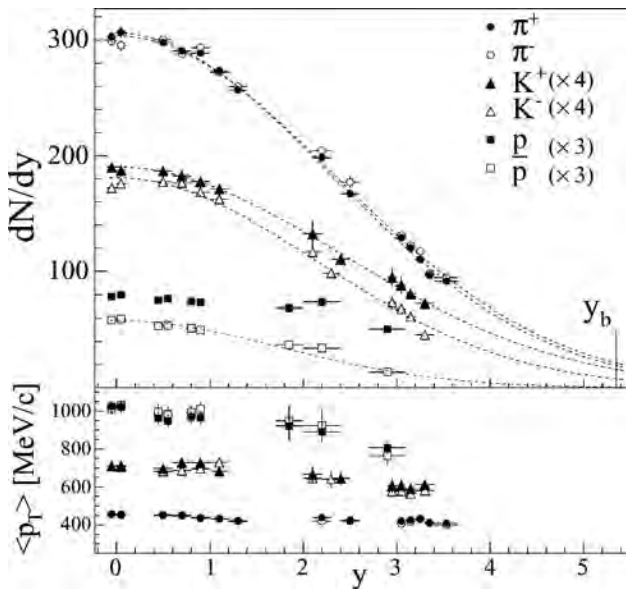


FIGURE 4. π , K and p rapidity densities (upper panel) and mean transverse momenta $\langle p_t \rangle$ (lower panel) for Au+Au at $\sqrt{s_{NN}} = 200$ GeV.

There is also an increasing production of K^+ over K^- as the forward rapidity region is approached. The lower panel shows the average transverse momenta of the identified particles. There is no significant difference between the particles and their anti-particles with respect to p_t . With increasing rapidity, there is a slight decrease in $\langle p_t \rangle$

4. Quark Chemistry

Anti-particle to particle ratios can yield important information on the dynamics of reaction mechanisms in large systems [9, 10]. The rapidity densities shown in Fig. 4 can be used directly to extract ratios of the different particle species. In Fig. 5 we show such anti-particle to particle ratios [11] for the π , K and p as a function of rapidity for the top 20%

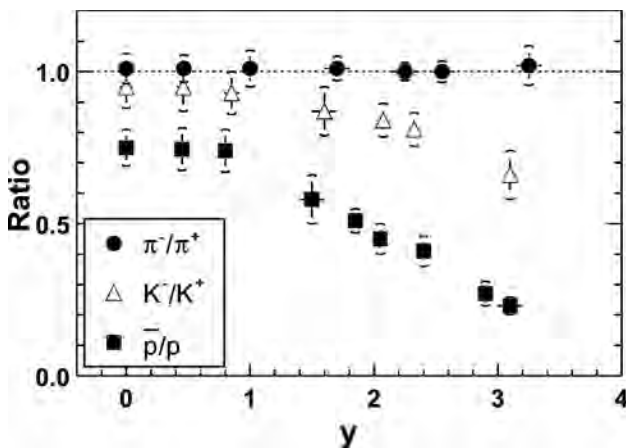


FIGURE 5. Anti-hadron to hadron ratios as a function of rapidity in $^{197}\text{Au} + ^{197}\text{Au}$ at $\sqrt{s_{NN}} = 200$ GeV for the top 20% central collisions.

central collisions. We see, as noted above, that the pion ratios remain close to unity over the entire rapidity range measured. The K^-/K^+ ratios, however, show a decrease from 0.95 ± 0.05 near mid-rapidity to 0.67 ± 0.06 at $y \sim 3$. The K^-/K^+ and \bar{p}/p ratios are roughly constant in the interval of $0 < y < 1$. The \bar{p}/p ratios, nearly constant at about 0.75 for $y < 1$, show a decrease to about 0.2 at the most forward rapidity studied. The value of $\bar{p}/p \sim 0.75$ at mid-rapidity corresponds to the largest ratio of anti-matter to matter observed to date in heavy ion collisions in the laboratory and indicates that a state of near net-baryon free matter has been created.

The ratio data at mid-rapidity have been analyzed in terms of a thermal model [12] where a proposed parameterization as a function of energy leads to a prediction for $\sqrt{s_{NN}} = 200$ GeV of $T \sim 177$ MeV and a baryo-chemical potential, $\mu_B \sim 30$ MeV. The small value of μ_B indicates a small net baryon density at mid-rapidity consistent with the fact that the \bar{p}/p ratio is large and close to 1.

A comparison of the K^-/K^+ and \bar{p}/p ratios also shows a remarkable correlation over the entire rapidity range we have measured as seen in Fig. 6. The figure also shows the results from BRAHMS at $\sqrt{s_{NN}} = 130$ GeV [13] as well as those of similar measurements made at AGS [14] and SPS [15, 16] energies. In a grand canonical approach where the strange quark chemical potential, μ_s , is fixed by conservation of strangeness [17], the antiparticle to particle ratios are controlled by the light and strange quark fugacities, $\lambda_q = e^{\mu_q/T}$ and $\lambda_s = e^{\mu_s/T}$. This leads to the prediction that

$$\frac{K^-}{K^+} = e^{2\mu_s/T} e^{-2\mu_q/T} = e^{2\mu_s/T} \left(\frac{\bar{p}}{p} \right)^{\frac{1}{3}} \quad (2)$$

which reduces to

$$\frac{K^-}{K^+} = \left(\frac{\bar{p}}{p} \right)^{\frac{1}{3}} \quad (3)$$

for $\mu_s = 0$. This dependence is shown as the dotted line in Fig. 6. We see that this simple equation slightly underpredicts the data suggesting non-zero strangeness.

The solid line in figure 6 shows the prediction of the grand canonical calculation [18] for a constant temperature of 170 MeV. These results suggest in the context of these models that the baryon chemical potential evolves from about $\mu_B \approx 130$ MeV at $y \sim 3$ to $\mu_B \approx 30$ MeV at mid-rapidity.

5. Nuclear Stopping

Another measurement where the unique extensive coverage of BRAHMS is crucial is that of nuclear stopping. We have deduced the stopping in $^{197}\text{Au} + ^{197}\text{Au}$ at $\sqrt{s_{NN}} = 200$ GeV by measuring the net-proton dN/dy from mid-rapidity to $y \sim 3$ and, from that, estimating the net-baryon dN/dy [19]. The net-baryon dN/dy is shown in Fig. 7 in the inset. The

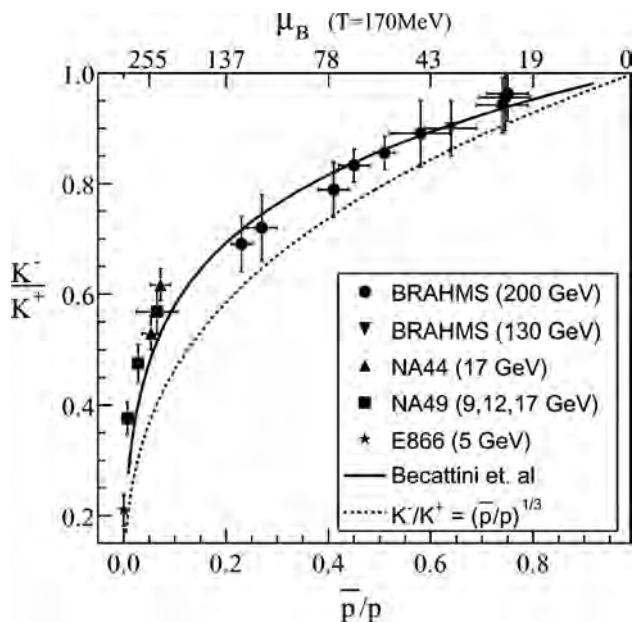


FIGURE 6. K^-/K^+ vs \bar{p}/p ratios. Dark solid symbols indicate the BRAHMS results in $^{197}\text{Au} + ^{197}\text{Au}$ at $\sqrt{s_{NN}} = 200$ GeV and 130 GeV from reference [13]. Light solid symbols show lower energy data [14–16]. The solid line shows the results of Becattini's model [18] and the dashed line shows the ansatz given in the inset. The baryon chemical potential, μ_B , shown on the top scale is in MeV.

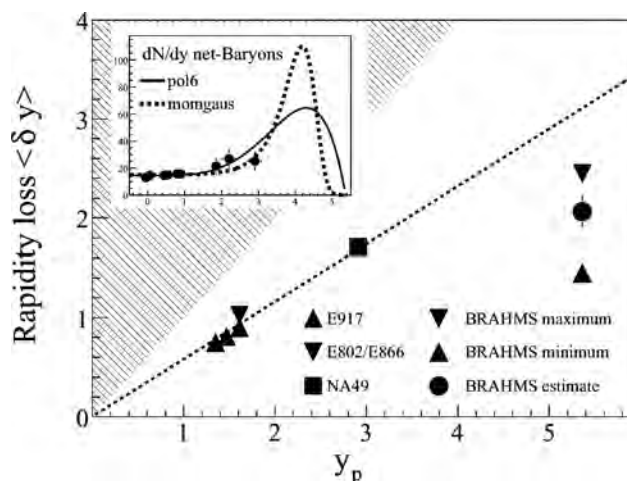


FIGURE 7. Rapidity loss using equation 5 as a function of projectile rapidity in the center of mass. The hatched area indicates the unphysical region and the dashed line shows phenomenological scaling $\langle \delta y \rangle = 0.58 y_p$ extracted from lower energy data [20–22]. Inset: Extrapolated net baryon distribution with different fits to the data (see text).

dashed line shows a fit to the measured data using a Bjorken inspired symmetric sum of 2 Gaussians in momentum space

$$\Sigma_{\pm} \exp \frac{-(p_z \pm \langle p_z \rangle)^2}{2\sigma_{p_z}^2} \quad (4)$$

where $p_z = m_N \sinh(y)$, assuming $p_t \sim 0$, and the solid curve shows a fit to a 6th order polynomial. The fits are con-

strained by the fact that the total baryon number, the integral under each curve, must be conserved and equal to $\langle N_{part} \rangle$, the average number of participating nucleons in the collision. From the fits, the rapidity loss can be determined using

$$\langle \delta y \rangle = y_p - \langle y \rangle = y_p - \frac{2}{\langle N_{part} \rangle} \int_0^{y_p} y \frac{dN_{(B-\bar{B})}}{dy} dy \quad (5)$$

The resultant $\langle \delta y \rangle \approx 2.0$ is shown as a solid circle in Fig. 7 along with the systematics of data from other energies [20–22]. The dashed line shows phenomenological scaling, $\langle \delta y \rangle = 0.58 y_p$, extracted from lower energy data [20–22]. The error bars at $y_p = 5.4$, the rapidity of the beam at $\sqrt{s_{NN}} = 200$, represents the difference between the two different fits. Clearly the constraint on the baryon-number ensures an accurate determination even though we did not measure up to the beam rapidity.

The lower energy data shown in figure 7 exhibit a linear relationship with y_p through SPS energies, $\langle \delta y \rangle = 0.58 y_p$. This scaling is broken, however, at $\sqrt{s_{NN}} = 200$ GeV. Assuming even the extreme conditions that the non measured baryons are either at the edge of the BRAHMS acceptance or at the beam rapidity leads to the data points represented by the triangles near the beam rapidity. The assumption of these extreme conditions does not follow the scaling systematics observed at the lower energies.

The energy loss can be determined using the total energy per net-baryon:

$$E = \frac{1}{\langle N_{part} \rangle} \int_{-y_p}^{y_p} \langle m_T \rangle \cdot \cosh y \cdot \frac{dN_{(B-\bar{B})}}{dy} \cdot dy. \quad (6)$$

resulting in 27 GeV which leads to an energy loss of 73 GeV out of the initial 100 GeV per participant, ie $\Delta E = 25.7$ TeV in total for central collisions.

6. High p_t Suppression

The Quark Gluon Plasma (QGP) is expected to be a dense medium of free color charges where, among other things, fast partons may undergo energy loss by gluon bremsstrahlung. One way to search for signals of a dense medium is to determine whether observables of elementary nucleon-nucleon collisions from heavy ion collisions appear to reflect simple binary scaling of elementary nucleon-nucleon collisions or whether medium effects may be at work. A variable typically used to test nucleon-nucleon scaling is the nuclear modification factor, R_{AA} , defined as:

$$R_{AA} = \frac{1}{\langle N_{coll} \rangle} \frac{d^2 N^{AA}/dp_t dy}{d^2 N_{inel}^{pp}/dp_t dy}. \quad (7)$$

where N_{coll} is the average number of binary collisions in the $A + A$ event. R_{AA} is a measure of how much the nucleus-nucleus collisions deviate from simple nucleon-nucleon scaling. A value of $R_{AA} \sim 1$ indicates that nucleus-nucleus collisions are simply the superposition of elementary nucleon-nucleon collisions while suppressions or enhancements relative to unity may signal medium effects. For example in Pb

+ Pb collisions at $\sqrt{s_{NN}} = 17$ GeV [23–25], R_{AA} was observed to be larger than one for $p_t > 1.5$ GeV/c. This was attributed to multiple scattering of partons in the initial stage of the reaction (the Cronin effect) [26].

Another variable which provides similar information, but does not depend on a measurement of the elementary reference spectra, is R_{cp} . It is defined as

$$R_{cp} = \frac{\frac{1}{\langle N_{coll}^{cent} \rangle} d^2 N^{cent} / dp_t dy}{\frac{1}{\langle N_{coll}^{perip} \rangle} d^2 N^{perip} / dp_t dy} \quad (8)$$

It is based on the expectation that any nuclear modification in peripheral collisions is not significant.

For our Au+Au data, Fig. 8 shows R_{AA} for charged hadrons as a function of p_t [27]. The data used for the elementary reference was the $p + \bar{p}$ data of reference [28]. We observe in the top panel of figure 8 that for the 0-10% most central collisions, R_{AA} is significantly below the value expected for simple binary scaling (unity; indicated by the dashed line in Fig. 8) for $p_t > 2$ GeV both at mid-rapidity (left panel) and at $\eta \sim 2.2$ (right panel). This could be indicative of a dense medium as higher p_t particles would be slowed and would show up at lower p_t . The ratios for $p_t < 2$ GeV are dominated by soft collisions and therefore expected to scale by the number of participants, N_{part} . The expected

value for N_{part} scaling is shown as the dotted lines in Fig. 8. The center panels of figure 8 shows R_{AA} for 40-60% central collisions. The value of R_{AA} is ~ 1 for $p_t > \sim 1.5$ GeV/c indicating a smaller volume and possibly a less dense medium for the less violent (more peripheral) collisions. The value near one also justifies the use of R_{cp} (equation 8) because we observe that the nuclear modification is, in fact, not significant for the peripheral collisions.

The bottom panels show R_{cp} as a function of p_t for the 0-10% central collisions. We observe the values are significantly below unity leading to the same conclusion as shown with R_{AA} for the central collisions.

To interpret Fig. 8 as evidence of a dense medium produced in the most violent $^{197}\text{Au} + ^{197}\text{Au}$ collisions, it must be verified that initial state effects, such as gluon saturation in the collisions partners, are not responsible for the suppression. To test this, BRAHMS (as well as the other three RHIC experiments) measured R_{dA} for $d + ^{197}\text{Au}$ at $\sqrt{s_{NN}} = 200$ GeV where no final state deconfined medium is expected to be present. The R_{dA} results from our experiment are shown as triangles in Fig. 9. We observe that R_{dA} is significantly larger than one at $p_t > 2$ GeV/c in contrast to R_{AA} from $^{197}\text{Au} + ^{197}\text{Au}$ (solid circles; same as left top panel of figure 8). This shows clearly and unambiguously that the R_{AA} for $^{197}\text{Au} + ^{197}\text{Au}$ at $\sqrt{s_{NN}} = 200$ results from mostly final state effects and not initial state effects, providing convincing evidence for production of a heretofore unknown dense medium. The other three RHIC experiments reached similar conclusions [29–31] and these observations the strongest evidence yet of the existence of a hot, dense state of matter with free color charges.

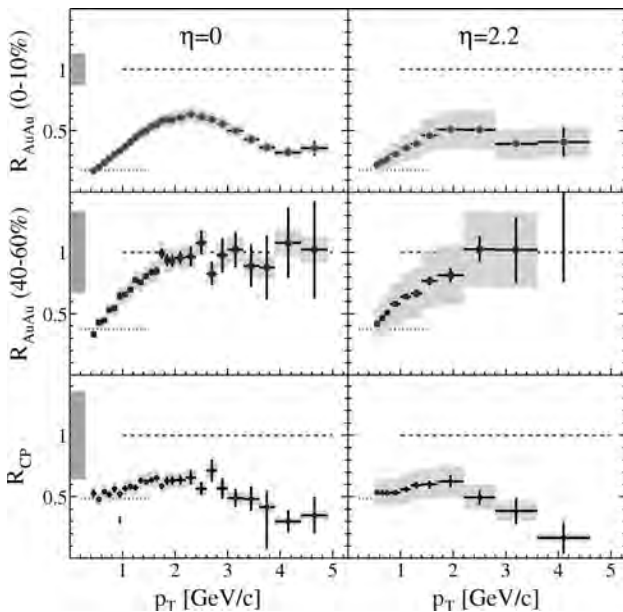


FIGURE 8. Top: Nuclear modification factors, R_{AA} as a function of p_t for $^{197}\text{Au} + ^{197}\text{Au}$ at $\sqrt{s_{NN}} = 200$ GeV at mid-rapidity (left) and $\eta = 2.2$ (right) for the 0-10% most central collisions. Center: Same as top, but for centrality of 40-60%. Bottom: R_{cp} as a function of p_t using the 0-10% vs 40-60% collision centralities. The dotted and dashed lines show the values of R_{AuAu} expected if scaling by the number of participants or by the number of binary collisions, respectively. The gray bands show the estimated systematic errors.

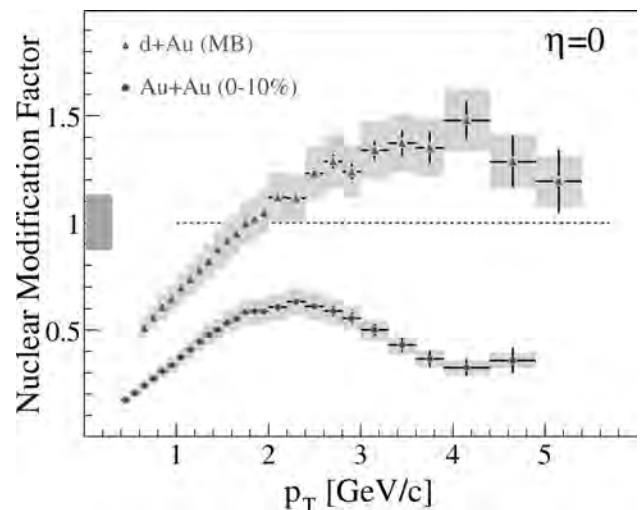


FIGURE 9. Nuclear modification factor for minimum bias $d + ^{197}\text{Au}$ collisions at $\sqrt{s_{NN}} = 200$ GeV (solid triangles) compared to central Au+Au collisions (solid circles).

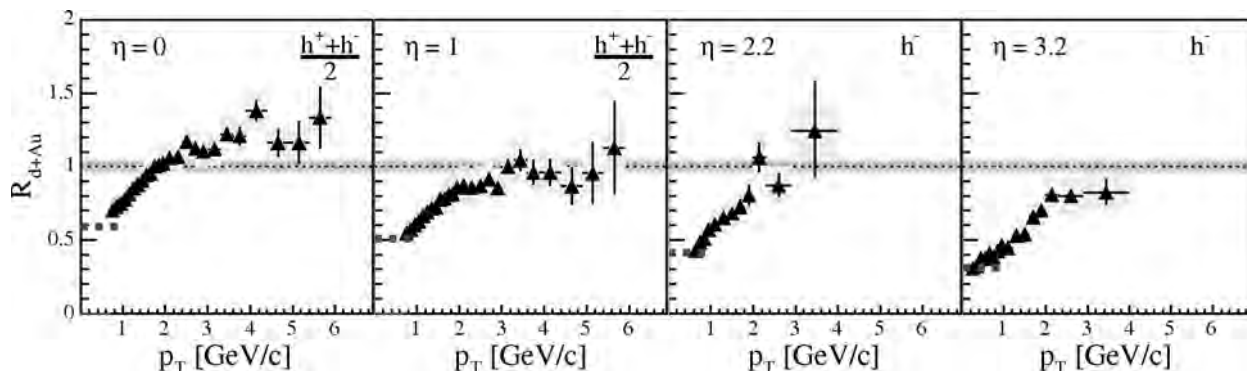


FIGURE 10. Nuclear modification factors from $d+^{197}\text{Au}$ collisions for charged hadrons for different pseudo-rapidities.

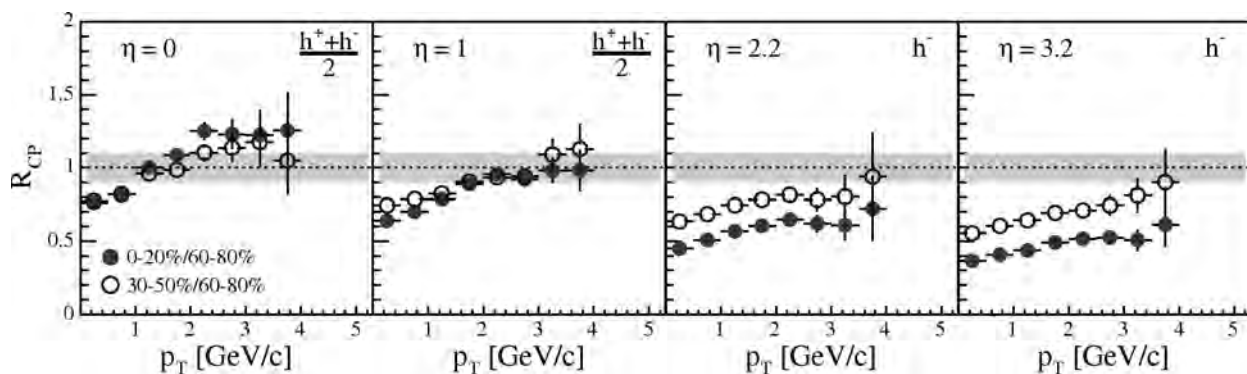


FIGURE 11. R_{cp} for central (full points) and semi-central (open points) $d+^{197}\text{Au}$ collisions as a function of pseudo-rapidity.

7. High p_t suppression in $d+^{197}\text{Au}$

We observed in Fig. 9 that R_{dA} for $d+^{197}\text{Au}$ at $\sqrt{s_{NN}}=200$ is significantly above one reflecting the long established Cronin effect [26]. Recall that R_{AA} for $^{197}\text{Au} + ^{197}\text{Au}$ shows suppression at $\eta \sim 2.2$. We have investigated the rapidity dependence of R_{dA} of $d + ^{197}\text{Au}$ [32]. In Fig. 10 we show the rapidity dependence of R_{dA} from mid-rapidity (left panel) to $\eta \sim 3$ in the right panel. There is a clear evolution toward increasing suppression with rapidity. It has been proposed that this effect is related to the possible existence of the Color Glass Condensate (CGC) [33], a description of the initial ground state of the nuclei prior to collisions where the number of gluons with low $x = (m_T/\sqrt{s_{NN}})e^{-y}$ are depleted due to gluon fusion.

We also investigate the centrality dependence using the R_{cp} factors. Figure 11 shows the rapidity evolution for two sets of R_{cp} , central (0-10%) vs. peripheral (60-80%) (closed points) and semi-central (30-50%) vs. peripheral (60-80%) (open points). We see the enhancement at mid-rapidity consistent with R_{dA} in figure 10. This evolves toward suppression as the pseudorapidity increases to $y \sim 3$. In addition, the central R_{cp} values show slightly more enhancement at mid-rapidity while the two R_{cp} are roughly equal and near to one at $\eta = 1$. From that point the more central R_{cp} exhibits more suppression as pseudorapidity increases. This suggests that the suppression mechanism is more efficient at higher centrality.

Such a suppression has been qualitatively predicted by several authors [34–37] within the Color Glass Condensate picture and indicates that an initial state effect may become dominant at forward rapidities. Recently a more quantitative framework for the CGC has been developed [38] by including realistic parton wave-functions along with valence quarks. In reference [38] the authors are able to obtain fairly quantitative agreement with our data, both in the magnitude of R_{dA} and in the magnitude and centrality dependence of R_{cp} .

8. Summary

Measurements from BRAHMS have yielded a plethora of new results, especially in the forward region. These results are anchored by measurements of identified particle spectra over a large rapidity range, $0 < y < 3.2$. From this we obtained yields which led to a deduction of stopping and energy loss. Results from these measurements were used to interpret particle multiplicities from global detectors. The energy density was estimated to be $\epsilon \approx 5 \text{ GeV}/\text{fm}^3$, a value that exceeds by a factor of 5 QCD predictions for the energy threshold for quark gluon plasma production. Measurements of \bar{p}/p ratios show the creation of the largest ratio of anti-matter to matter yet observed in heavy ion reactions and indicates a near baryon-free region at mid-rapidity. Correlations of K^-/K^+ to \bar{p}/p show a seemingly universal relationship. From that we are able to estimate baryo-chemical potential as well as

a limit on strangeness content. Thermal model calculations using a temperature of 170 MeV fit these correlations well. Studies of high p_t suppression in $^{197}\text{Au} + ^{197}\text{Au}$ at mid-rapidity established a new final state of dense matter. The p_t suppression pattern in $d + ^{197}\text{Au}$ is consistent with the existence of the Color Glass Condensate, a description of the ground state of nuclei prior to collisions. Both initial and final state suppression mechanisms may simultaneously be present in central Au + Au collisions at forward rapidity.

All of these conclusions depend upon the results at forward angles for their interpretation. There are many new data currently under analysis, notably for $^{197}\text{Au} + ^{197}\text{Au}$ at

$\sqrt{s_{NN}} = 62$ GeV, which also benefit from our broad measurement capability. In addition the next RHIC run with Cu+Cu at $\sqrt{s_{NN}} = 200$ GeV will add results in an intermediate mass region to the already impressive results.

Acknowledgements

This work was supported by the United States Department of Energy under Grant # DE-FG03-93ER40773, the Danish Natural Science Research Council, the Research Council of Norway, the Polish State Committee for Scientific Research (KBN) and the Romanian Ministry of Research.

* Speaker and corresponding author email:
hagel@comp.tamu.edu.

1. M. Adamczyk *et al.*, BRAHMS Collaboration, Nucl. Instr. Meth. A **499** (2003) 437.
2. I. G. Bearden *et al.*, BRAHMS Collaboration, Phys. Lett. **B523** (2001) 227.
3. I. G. Bearden *et al.*, BRAHMS Collaboration, Phys. Rev. Lett. **88** (2002) 202301.
4. J. D. Bjorken, Phys. Rev. D **27** (1983) 140.
5. F. Karsch, Nucl Phys **A698** (2002) 199.
6. M. Gyulassy and T. Matsui, Phys Rev. D **29** (1984) 419.
7. P. Deines-Jones *et al.*, Phys. Rev. C **62** (2000) 014903.
8. J. Benecke *et al.*, Phys. Rev. **188** (1969) 2159.
9. N. Herrmann *et al.*, Ann. Rev. Nucl. Part. Sci. **49** (2000) 581.
10. H. Satz, Rep. Prog. Phys. **63** (2000) 1511.
11. I. G. Bearden *et al.*, Phys. Rev. Lett. **90** (2003) 102301.
12. P. Braun-Munzinger *et al.*, Phys. Lett. **B518** (2000) 41.
13. I. G. Bearden *et al.*, Phys. Rev. Lett. **87** (2001) 112305.
14. L. Ahle *et al.*, E866 Collaboration, Phys. Rev. Lett. **81** (1998) 2560 and Phys. Rev. C **60** (1999) 044904.
15. Y. Afanasiev *et al.*, NA49 Collaboration, nucl-ex/0205002; J. Bächler *et al.*, Nucl. Phys. **A661** (1999) 45.
16. I. G. Bearden *et al.*, NA44 Collaboration, J. Phys. G, Nucl. Part. **23** (1997) 1865.
17. J. Rafelski, Phys. Lett. **B262** (1991) 333.
18. F. Becattini *et al.*, Phys. Rev. C **64** (2001) 24901.
19. I. G. Bearden *et al.*, Phys. Rev. Lett **93** (2004) 102301.
20. F. Videbaek and O. Hansen, Phys. Rev. C **52** (1995) 2684.
21. B. Hong *et al.*, FOPI Collaboration, Phys. Rev. C **57** (1998) 244; **58** (1998) 603.
22. B. B. Back *et al.*, E917 Collaboration, Phys. Rev. Lett. **86** (2001) 1970.
23. M. M. Aggarwal *et al.*, Eur. Phys. J. **C18** (2001) 651.
24. H. Appelshauser *et al.*, Phys. Rev. Lett. **82** (1999) 2471.
25. G. Agakishiev *et al.*, hep-ex/0003012.
26. J. W. Cronin *et al.*, Phys. Rev. D **11** (1975) 3105.
27. I. Arsene *et al.*, Phys. Rev. Lett. **91** (2003) 072305.
28. C. Albajar *et al.*, Nucl. Phys. **B335** (1990) 261.
29. B. B. Back *et al.*, Phys. Rev. Lett. **91** (2003) 072302.
30. J. Adams *et al.*, Phys. Rev. Lett. **91** (2003) 072304.
31. S. S. Adler *et al.*, Phys. Rev. Lett. **91** (2003) 072303.
32. I. Arsene *et al.*, Phys. Rev. Lett **93** (2004) 242303.
33. D. Kharzeev *et al.*, Phys Lett **B561** (2003) 93.
34. A. Dumitru *et al.*, Phys. Lett. **B547** (2002) 15.
35. J. Jalilian-Marian *et al.*, Phys. Lett. **B577** (2003) 54; A. Dumitru *et al.*, Phys. Rev. Lett **89** (2002) 022301.
36. R. Baier *et al.*, Phys. Rev. D **68** (2003) 054009.
37. D. Kharzeev *et al.*, Phys. Rev. D **68** (2003) 094013; D. Kharzeev *et al.*, Phys. Lett. **B561** (2003) 93.
38. D. Kharzeev *et al.*, Phys. Lett. **B599** (2004) 23.